How erosive are submarine landslides?

Harya D. Nugraha[1,2,*], Christopher A-L. Jackson[1], Howard D. Johnson[1], David M. Hodgson[3] and Michael A. Clare[4]

[1]*Basins Research Group (BRG), Department of Earth Science and Engineering, Imperial College, London SW7 2BP, UK*

[2]*Universitas Pertamina, Jakarta 12220, Indonesia*

[3]*School of Earth and Environment, University of Leeds, Leeds LS2 9JT, UK*

[4]*National Oceanography Centre, Southampton SO14 3ZH, UK*

*E-mail: harya.nugraha14@imperial.ac.uk

ABSTRACT

Submarine landslides (slides) are ubiquitous on continental margins. They can pose a major hazard by triggering tsunami and damaging essential submarine infrastructure. Slide volume, which is a key parameter in hazard assessment, can change after initiation through substrate and/or water entrainment. However, the erosive capacity of slides is uncertain. Here, we quantify slide erosivity by determining the ratio of deposited (Vd) to initially evacuated (Ve) sediment volumes. Slides that gain volume through erosion = Vd/Ve>1. We apply this method to a large (500 km^3), seismically imaged slide offshore NW Australia, and review Vd/Ve ratios for other large slides worldwide. Nine of the 11 slides have Vd/Ve>1 (median value=2), showing that emplaced volumes increased after initial failure. The Gorgon Slide is the most erosive slide currently documented (Vd/Ve=13), possibly reflecting its passage across a highly erodible carbonate ooze substrate. This new approach to quantifying erosion is important for hazard assessments as substrate-flow interactions control slide speed and run-out distance. The variations in slide volume

also have important implications for submarine infrastructure impact assessments, including more robust tsunami modelling.

INTRODUCTION

Submarine landslides (slides) are key components of many deep-water successions, with individual deposits comprising volumes of >10,000 km^3 (e.g. Moscardelli and Wood, 2016). Slides can be tsunamigenic, such as in Papua New Guinea where a slide triggered a tsunami that killed >2000 people (Tappin et al., 2001). Slides can also damage vital seabed infrastructure, such as the global network of telecommunication cables (Carter et al., 2014), and hydrocarbon pipelines (e.g. Randolph and White, 2012). Most studies have focused on siliciclastic slides (e.g. Moscardelli and Wood, 2016; Ten Brink et al., 2006), although carbonate ooze comprises a significant portion (c.30%) of the world's ocean floor (see Appendix DR1, Dutkiewicz et al., 2015). Such oozes have different mechanical properties to siliciclastic sediments; i.e. the post-failure shear strength of an ooze can be as low as 10% of its original strength, compared to 55% for siliciclastic clay (Gaudin and White, 2009). Slides involving carbonate ooze-dominated seabeds may thus be more erosive (Winterwerp et al., 2012), possibly with a greater potential impact on offshore infrastructure and a higher tsunamigenic potential.

A slide may translate across the substrate on a thin lubricating basal layer ('hydroplaning'; e.g. Mohrig et al., 1998). Such slides may be non-erosive, and may even suffer volume loss due to partial flow transformation from debris flow to turbidity current (e.g. Sun et al., 2018). Although field data provide evidence for substrate deformation and entrainment during slide transport (e.g. Sobiesiak et al., 2018), the scale, geometry, and style of these erosional processes are most readily identified in 3D seismic reflection data (e.g. grooves and striations; e.g. Gee et al., 2005; ramps; e.g. Bull et al., 2009; downslope-diverging peel-back scours; e.g. Sobiesiak et al., 2018; substratederived megaclasts; e.g. Hodgson et al., 2018). Despite widespread evidence for erosion, the amount of substrate entrainment during slide transport is poorly constrained. This partly reflects limited exposure of exhumed slides in the field, and poor imaging by and/or limited coverage of subsurface data. Quantifying erosivity is important because: 1) entraining material during transport via basal erosion could modify slide rheology and thus affect its speed and run-out distance; two key parameters for both tsunami modelling and impact assessments on submarine infrastructures (e.g. Bruschi et al., 2006); and 2) initial failed volume is a key parameter in tsunami modelling (e.g. Murty, 2003).

Here, we use 3D seismic reflection data from the Exmouth Plateau, offshore NW Australia to quantify the erosivity of the Gorgon Slide (Fig. 1). This study focuses on the discrepancy between the volumes of evacuated (Ve) and deposited (Vd) sediments. We introduce a new measure (Vd/Ve ratio) to provide a first-order estimate of slide erosivity, where Vd/Ve>1 indicates substrate entrainment during transport (see Dataset and Methods). We also review other slides for which Vd and Ve are presented (e.g. Moscardelli and Wood, 2016). Our approach: 1) provides insights into the likely physical processes occurring during slide transport; 2) may help improve prediction of the impact of slides on submarine infrastructure; and 3) better constrain slide-induced tsunami numerical models.

GEOLOGICAL SETTING

The post-rift (Late Cretaceous-present) history of the Exmouth Plateau (Fig. 1A) is dominated by carbonate ooze deposition (Longley et al., 2002). Miocene intra-plate shortening and folding promoted slope steepening across the plateau and present-day shelf (Keep et al., 1998). Associated seismicity caused elevated fluid pressures, which triggered slope failure and the transport of multiple slides around the plateau and shelf (e.g. Scarselli et al., 2013). Here we focus on the most recent slide (Gorgon Slide Fig. 1B-C).

DATASET AND METHODS

We analyse five time-migrated 3D seismic reflection datasets (Fig. 1) that image both the evacuation and deposition zones of the Gorgon Slide and the adjacent, unfailed continental slope (Fig. 1B-C). Given a near seabed sediment velocity of 1824 m/s, and a dominant seismic frequency of 40-60 Hz, the estimated vertical seismic resolution at the base of the Gorgon Slide (c.500 m below seabed) ranges from 8-11 m. The 3D seismic volumes have bin spacings of 12.5 x 18.75 m and 20 x 25 m (see Appendix DR2 for details). Maps of the present seabed and base of the Gorgon Slide (see Fig. 1D-E) were converted from time to depth using average water velocity (1519 m/s) and average near seabed sediments velocity (1824 m/s), respectively (Appendix DR2). Ten industry wells constrain the water velocity (Fig. 1B). Well ODP 762, located c. 200 km NW of our seismic datasets, penetrated a similar seismic-stratigraphic sequence to that encountered in the study area; we therefore used data from this well to infer near seabed lithology and its physical properties (e.g. velocity and porosity; Fig. 1A).

We calculate the ratio between the volume of the slide evacuation zone (Ve) and the slide deposit itself (Vd) to derive a first-order estimation of slide erosivity (Fig. DR3A). When $Vd/Ve<1$, we infer the slide loses volume during transport; this could reflect partial flow transformation from debris flow to turbidity current, resulting in deposition beyond the slide margin (Fig. DR3B). When Vd/Ve=1, we infer no net volume change from the initial failed mass (e.g. entrained sediment volume balanced by volume loss due to flow transformation) (Fig. DR3C). Finally, Vd/Ve>1 indicates net volume gain during transport, suggesting lengthening and/or deepening of the basal-shear surface, plus substrate entrainment (Fig. DR3D).

We calculated the Vd/Ve ratio for the Gorgon Slide using three established methods; (i) theoretical volume method - this assumes that Ve and Vd have a wedge-shaped (McAdoo et al., 2000), half-ellipsoid geometry (e.g. Wilson et al., 2004), respectively; (ii) bulk volume method – this estimates Ve by calculating the volume between present-day and interpreted pre-failure seabed within the evacuation zone, whereas Vd is obtained by calculating the volume of the deposit between the basal-shear surface and top surface (e.g. Piper et al., 1997); and (iii) compacted volume method – this is similar approach to method (i), but counts only the solid-state sediment fraction, removing water and pore-space (i.e. theoretical zero-porosity) (e.g. Lamarche et al., 2008) (Appendix DR4). Despite the uncertainties associated with each method, Vd/Ve ratio provides a first-order estimation of slide erosivity.

EROSIVITY OF SUBMARINE LANDSLIDES

The Gorgon Slide

The source area for the Gorgon Slide is defined on its updip margin by a steep headwall scarp. The slide travelled c. 70 km north-westwards from an evacuation zone, accumulating in a downdip deposition zone (Fig. 1D). The slide deposit is c.30 km-wide, thickens downslope to c.500 m, and covers a total area of 1760 km^2. Transparent, chaotic seismic reflections likely reflect debritic material forming the slide matrix (Fig. 1D-E) (e.g. Posamentier and Martinsen, 2011). Packages of subparallel, high-amplitude reflections encased in this matrix are likely megaclasts

(Fig. 1E) (e.g. Jackson, 2011), either sourced from the evacuation zone or entrained from the substrate. Further evidence of basal erosion is shown by truncation of underlying reflections (Fig. 1E).

The Vd of the Gorgon Slide was calculated using the basal-shear surface and seabed (see Fig. 1D-E). This represents a minimum value because a small part (c.7%; i.e. 166 km^2 of 1760 km^2, see Fig. 1C) of the slide is not imaged within the seismic dataset. The headwall scarp of the slide extends from a lateral scarp in the SW to, at least, a gullied slope in the NE (Fig. 2A-C). The headwall scarp may also extend NE outside of the available dataset given it is difficult to confidently identify a lateral scarp (such as in Fig. 2B). However, we argue the NE lateral scarp is unlikely to lie beyond the seismically-imaged area given that numerous grooves lie along the basal shear surface and record erosion. Also, the deposit's lateral margin connects directly back to its source area, suggesting the NE-limit of the headwall scarp lies close to the gullied slope (Fig. 2A and C) (see also Hengesh et al., 2013, their Fig. 8). To capture this uncertainty, Ve estimations comprise both minimum (Fig. 2A) and maximum (Fig. 2D) cases related to the northeastern extent of the headwall scarp (see Appendix DR5). Ve was estimated by using the adjacent unfailed slope as a proxy for the pre-failure physiography across the evacuation zone (Fig. 3). The estimated Vd/Ve ratio for the Gorgon Slide ranges from 5-16, depending on the calculation method used and the headwall scarp extension uncertainties (see Appendix DR5). All methods suggest the slide was strongly erosive (i.e. Vd/Ve>1), an observation consistent with the abundant evidence for seismic-scale erosion along the basal-shear surface.

Global Analysis of Slide Erosivity

In order to place our results in a global context, we collated data from other slides (see Appendix DR6). Of the 357 slides documented in 97 papers, only 11 had presented both Ve and

Vd. 9 of these 11 slides were erosive (Vd/Ve>1, with a median value of 2; Fig. 4). On average, the documented slides had final preserved slide volume as much as three times the initial failed volume. The Gorgon Slide (Vd/Ve=5-16) is the most erosive slide yet documented (Fig. 4B).

Although most are erosive, two slides have Vd/Ve<1 (Fig. 4B): 1) in the South China Sea, where volume loss is attributed to partial flow transformation from debris flow to turbidity current, resulting in (sub-seismic resolution) turbidites beyond the main slide pinchout, and pore volume reduction due to continuous shearing during transport (i.e. shear compaction) (Sun et al., 2018); and 2) in New Zealand, the Ruatoria Debris Avalanche, where the evacuation zone was formed by a combination of slope failure *and* tectonic erosion due to seamount subduction (i.e. not solely related to flow processes during transport) (Collot et al., 2001).

DISCUSSION

Large submarine landslides are predominantly erosive

We show that slide deposit volumes are typically larger than the initial failed volume, thereby confirming the erosivity of their parent flows (Fig. 4). Substrate entrainment and volume gain occurs when the shear stress exerted by the overriding parent flow exceeds the shear strength of the substrate. The overriding flow may elevate pore pressures in the shallow substrate, causing liquefaction or strain softening (e.g. Ortiz-Karpf et al., 2017), or substrate deformation (e.g. Butler and McCaffrey, 2010). Both mechanisms will reduce substrate strength, making it more susceptible to entrainment. Substrate entrainment can also occur due to 'tooling' by rigid blocks (e.g. megaclasts) to form tool marks, such as grooves and striations (e.g. Gee et al., 2005).

We plotted several commonly-measured slide parameters (i.e. evacuated volume, runout distance, height drop, and mobility) to investigate any potential relationship with slide erosivity (see Appendix DR7). We found no clear relationship between these parameters (R^2: 0.0002-0.05), suggesting they may have limited predictive power and that other, as-yet unknown, possibly local factors are at play. For example, slope gradient changes may control the degree of erosion; i.e. an abrupt decrease in slope gradient may increase the vertical impact of the parent flow on the substrate, resulting in more erosion and substrate entrainment (Ogata et al., 2014; see also Moernaut and De Batist, 2011).

We suggest that pre-failure substrate morphology and composition are more likely the primary factors controlling erosion. This is because substrate morphology may focus the parent flow, while its composition determines erosion patterns (Ortiz-Karpf et al., 2017). For instance, a clay-rich substrate is typically more resistant to erosion than a sandy substrate due to electrochemical forces between particles (e.g. Ortiz-Karpf et al., 2017). In the case of the Gorgon Slide, we note that, despite being locally erosive, the basal-shear surface broadly follows the morphology of underlying strata (Fig. 1E), and contains downslope-converging grooves on its basal-shear surface (Fig. 2D). The presence of grooves imply that the parent flow was focused on the northeastern-side of the slide, resulting in a straight, erosional lateral margin (see Fig. 1E and Fig. 2D).

The carbonate ooze substrate of the Gorgon Slide is dominated by fragile foraminifera and nannofossils, which become weakly cemented at their contacts during early burial. This preserves unusually high near-surface porosities and results in higher initial strength than (uncemented) siliciclastic sediments (von Rad et al., 1992). Under loading, these fragile biogenic particles are crushed, which generates excess near-seabed pore pressures and a dramatic loss of strength (e.g. Sharma and Joer, 2015). When carbonate oozes fail, their residual strength can be only 10% of their initial strength; compared to up to 55% for siliciclastic sediment (see Appendix DR8, Gaudin and White, 2009).

Volume *loss* during transport could occur due to entrainment of coarse-grained (e.g. sandy) sediments (e.g. Dykstra et al., 2011) and/or ambient water into the flow (e.g. Talling et al., 2012). For example, Sun et al. (2018) document a median volume loss of 86 km^3 (c.13.6% of Vd) for a slide in the South China Sea. They relate this to flow transformation from the parent debris flow into a slide-generated turbidity currents. Continuous shearing during transport may also have further reduced volume, given even a small shear stresses can cause fine-grained sediments to lose volume (Piper et al., 1997).

Implications of submarine landslides erosivity for geohazards assessments

Vd/Ve ratio provides a first-order, quantitative estimate of whether a slide increases or decreases its volume during transport. When a slide is erosive and ‘bulks-up’, its speed may decrease due to enhanced basal friction, thereby reducing run-out distance (e.g. Schulz et al., 2009). Conversely, when a slide hydroplanes and does not erode its substrate, both its transport speed and run-out distance may increase (e.g. Mohrig et al., 1998). Slide speed and run-out distance are thus key components for tsunami modelling (e.g. Murty, 2003), and for assessing the potential impact slides may have on submarine infrastructure (e.g. Bruschi et al., 2006). In addition, Ve is a key factor for tsunami modelling, as it dictates how much overlying water is displaced during failure (e.g. Murty, 2003). Accurate volume assessment is especially challenging if only Vd is known, and if there is significant erosion or partial flow transformation. For example, the use of Vd as an estimate of Ve for tsunami modelling will overestimate displacement of the overlying water when $Vd/Ve>1$. Conversely, if $Vd/Ve<1$, tsunami modelling will underestimate the displacement of the overlying water. Therefore, to understand uncertainties associated with tsunami modelling, a range of Vd/Ve scenarios should be considered. Our study suggests that most slides are erosive, and that a ratio of 1 to at least a median value of 2, should be used for the modelling. Carbonate ooze-dominated slides such as the Gorgon Slide, which are only very rarely documented, could also be significantly more erosive than siliciclastic slides.

ACKNOWLEDGEMENTS

We thank Geoscience Australia for providing seismic and borehole data, and Schlumberger are thanked for providing Petrel to Imperial College. The first author thanks the Indonesia Endowment Fund for Education (LPDP) (Grant No.: 20160822019161) for its financial support. MC was supported by the NERC National Capability CLASS Programme [Climate Linked Atlantic Sector Science Programme (No. NE/R015953/1)] and NERC Grant NE/T002034/1. We thank the editor, James Schmitt, and the reviewers (Matheus Sobiesiak, Joshu Mountjoy, and an anonymous reviewer), whose comments have helped to improve an earlier version of this manuscript.

REFERENCES CITED

Bruschi, R., Bughi, S., Spinazzè, M., Torselletti, E., and Vitali, L., 2006, Impact of debris flows and turbidity currents on seafloor structures: Norwegian Journal of Geology/Norsk Geologisk Forening, v. 86, no. 3.

Bull, S., Cartwright, J., and Huuse, M., 2009, A review of kinematic indicators from mass-transport complexes using 3D seismic data: Marine and Petroleum Geology, v. 26, no. 7, p. 1132-1151.

Butler, R., and McCaffrey, W., 2010, Structural evolution and sediment entrainment in mass-transport complexes: outcrop studies from Italy: Journal of the Geological Society, v. 167, no. 3, p. 617-631.

Carter, L., Gavey, R., Talling, P. J., and Liu, J. T., 2014, Insights into submarine geohazards from breaks in subsea telecommunication cables: Oceanography, v. 27, no. 2, p. 58-67.

Dutkiewicz, A., Müller, R. D., O'Callaghan, S., and Jónasson, H., 2015, Census of seafloor sediments in the world's ocean: Geology, v. 43, no. 9, p. 795-798.

Dykstra, M., Garyfalou, K., Kertznus, V., Kneller, B., Milana, J. P., Molinaro, M., Szuman, M., and Thompson, P., 2011, Mass-transport deposits: Combining outcrop studies and seismic forward modeling to understand lithofacies distributions, deformations, and their seismic stratigraphic expression: SEPM Special Publication, v. 96, p. 293-310.

Gaudin, C., and White, D., 2009, New centrifuge modelling techniques for investigating seabed pipeline behaviour, *in* Proceedings 17th International Conference on Soil Mechanics and Geotechnical Engineering, Alexandria, 2009, p. 448-451.

Gee, M., Gawthorpe, R., and Friedmann, J., 2005, Giant striations at the base of a submarine landslide: Marine Geology, v. 214, no. 1, p. 287-294.

Hengesh, J. V., Dirstein, J. K., and Stanley, A. J., 2013, Landslide geomorphology along the Exmouth Plateau continental margin, North West Shelf, Australia: Australian Geomechanics, v. 48, no. 4, p. 71-92.

Hodgson, D., Brooks, H., Ortiz-Karpf, A., Spychala, Y., Lee, D., and Jackson, C.-L., 2018, Entrainment and abrasion of megaclasts during submarine landsliding and their impact on flow behaviour: Geological Society, London, Special Publications, v. 477, p. SP477. 426.

Jackson, C. A., 2011, Three-dimensional seismic analysis of megaclast deformation within a mass transport deposit; implications for debris flow kinematics: Geology, v. 39, no. 3, p. 203-206.

Keep, M., Powell, C., and Baillie, P., 1998, Neogene deformation of the North West Shelf, Australia: The sedimentary basins of Western Australia, v. 2, p. 81-91.

Lamarche, G., Joanne, C., and Collot, J. Y., 2008, Successive, large mass-transport deposits in the south Kermadec fore-arc basin, New Zealand: The Matakaoa Submarine Instability Complex: Geochemistry, Geophysics, Geosystems, v. 9, no. 4.

Longley, I. M., Buessenschuett, C., Clydsdale, L., Cubitt, C. J., Davis, R. C., Johnson, M. K., Marshall, N. M., Murray, A. P., Somerville, R., and Spry, T. B., 2002, The North West Shelf of Australia - a Woodside Perspective, *in* Keep, M., and Moss, S. J., eds., The Sedimentary Basins of Western Australia 3: Petroleum Exploration Society of Australia Symposium: Perth, p. 28-88.

McAdoo, B., Pratson, L., and Orange, D., 2000, Submarine landslide geomorphology, US continental slope: Marine Geology, v. 169, no. 1, p. 103-136.

Moernaut, J., and De Batist, M., 2011, Frontal emplacement and mobility of sublacustrine landslides: results from morphometric and seismostratigraphic analysis: Marine Geology, v. 285, no. 1-4, p. 29-45.

Mohrig, D., Ellis, C., Parker, G., Whipple, K. X., and Hondzo, M., 1998, Hydroplaning of subaqueous debris flows: Geological Society of America Bulletin, v. 110, no. 3, p. 387-394.

Moscardelli, L., and Wood, L., 2016, Morphometry of mass-transport deposits as a predictive tool: GSA Bulletin, v. 128, no. 1/2, p. 47-80.

Murty, T., 2003, Tsunami wave height dependence on landslide volume: Pure and applied geophysics, v. 160, no. 10-11, p. 2147-2153.

Ogata, K., Pogačnik, Ž., Pini, G. A., Tunis, G., Festa, A., Camerlenghi, A., and Rebesco, M., 2014, The carbonate mass transport deposits of the Paleogene Friuli Basin (Italy/Slovenia): internal anatomy and inferred genetic processes: Marine geology, v. 356, p. 88-110.

Ortiz-Karpf, A., Hodgson, D. M., Jackson, C. A.-L., and McCaffrey, W. D., 2017, Influence of Seabed Morphology and Substrate Composition On Mass-Transport Flow Processes and Pathways: Insights From the Magdalena Fan, Offshore Colombia: Journal of Sedimentary Research, v. 87, no. 3, p. 189-209.

Piper, D. J. W., Pirmez, C., Manley, P. L., Long, D., Flood, R. D., Normark, W. R., and Showers, W., Mass Transport Deposits of the Amazon Fan, *in* Proceedings Ocean Drilling Program, Scientific Results1997, Volume 155, p. 109-146.

Posamentier, H. W., and Martinsen, O. J., 2011, The character and genesis of submarine mass-transport deposits: insights from outcrop and 3D seismic data: Mass-transport deposits in deepwater settings: Society for Sedimentary Geology (SEPM) Special Publication 96, p. 7-38.

Randolph, M. F., and White, D. J., 2012, Interaction forces between pipelines and submarine slides—A geotechnical viewpoint: Ocean Engineering, v. 48, p. 32-37.

Scarselli, N., McClay, K., and Elders, C., Submarine slide and slump complexes, Exmouth Plateau, NW Shelf of Australia, *in* Proceedings The Sedimentary Basins of Western Australia IV: Proceedings of the Petroleum Exploration Society of Australia Symposium, Perth, 2013.

Schulz, W. H., McKenna, J. P., Kibler, J. D., and Biavati, G., 2009, Relations between hydrology and velocity of a continuously moving landslide—evidence of pore-pressure feedback regulating landslide motion?: Landslides, v. 6, no. 3, p. 181-190.

Sharma, S., and Joer, H., Some characteristics of carbonate sediments from NorthWest Shelf, Western Australia, *in* Proceedings Frontiers in Offshore Geotechnics III: Proceedings of the 3rd International Symposium on Frontiers in Offshore Geotechnics (ISFOG 2015)2015, Volume 1, Taylor & Francis Books Ltd, p. 1109-1114.

Sobiesiak, M. S., Kneller, B., Alsop, G. I., and Milana, J. P., 2018, Styles of basal interaction beneath mass transport deposits: Marine and Petroleum Geology, v. 98, p. 629-639.

Sun, Q., Alves, T., Lu, X., Chen, C., and Xie, X., 2018, True volumes of slope failure estimated from a Quartenary mass-transport deposit in the northern South China Sea: Geophysical Research Letters.

Talling, P. J., Masson, D. G., Sumner, E. J., and Malgesini, G., 2012, Subaqueous sediment density flows: Depositional processes and deposit types: Sedimentology, v. 59, no. 7, p. 1937-2003.

Tappin, D., Watts, P., McMurtry, G., Lafoy, Y., and Matsumoto, T., 2001, The Sissano, Papua New Guinea tsunami of July 1998—offshore evidence on the source mechanism: Marine Geology, v. 175, no. 1-4, p. 1-23.

Ten Brink, U. S., Geist, E. L., and Andrews, B. D., 2006, Size distribution of submarine landslides and its implication to tsunami hazard in Puerto Rico: Geophysical Research Letters, v. 33, no. 11.

von Rad, U., Haq, B. U., Kidd, R. B., and O'Connell, S. B., 1992, Proceedings of the Ocean Drilling Program, Scientific Results, College Station, TX, Ocean Drilling Program.

Wilson, C. K., Long, D., and Bulat, J., 2004, The morphology, setting and processes of the Afen Slide: Marine Geology, v. 213, no. 1-4, p. 149-167.

Winterwerp, J., Kesteren, W., Prooijen, B., and Jacobs, W., 2012, A conceptual framework for shear flow–induced erosion of soft cohesive sediment beds: Journal of Geophysical Research: Oceans, v. 117, no. C10.

FIGURE CAPTIONS

Figure 1. A: Location of study area (EP: Exmouth Plateau; AR: Argo Abyssal Plain; GA: Gascoyne Abyssal Plain; CU: Cuvier Abyssal Plain). Yellow dot = location of ODP 762 well. B: Seabed time-structure map (top Gorgon Slide) showing slide evacuation and deposition zones. Red dots = wells used for depth conversion. C: Extent of the Gorgon Slide (grey). Blue dashed line defines the seismic-scale pinchout of the slide; c. 7% of the slide is not imaged by 3D seismic data but is mapped on 2D seismic profiles (green lines). Gorgon, Acme, Draeck, Duyfken, and Io-Jansz are the 3D seismic datasets were used in this study. D: NW-trending depositional dip-oriented seismic profile across the Gorgon Slide, showing cross-sectional view of the evacuation and deposition zones. E: NE-trending depositional strike seismic profile across the Gorgon Slide. Locations of seismic profiles are shown in B and C.

Figure 2. A: A three-dimensional perspective of present-day seabed showing lateral scarp in the SW and minimum extent of the headwall scarp marked by the presence of gullied slope. Grooves that can be traced back from the deposit to the source are also shown. B: Seismic profile across the lateral scarp limiting the headwall scarp in the SW. C: Seismic profile across a gully that may define the NE-limit of the headwall scarp, where no presence of scarp, indicating that this part of slope might not failed. D: A three-dimensional persepective of basal-shear surface showing downslope-converging grooves indicate that the parent flow was focused to the NE, and thus forming a straight, erosional lateral margin.

Figure 3. A: NW-trending seismic profile across the unfailed margin, just SW of the headwall scarp of the Gorgon Slide. B: Seabed depth-structure map showing the headwall scarp of the Gorgon Slide and the adjacent unfailed margin to the SW. C: NW-trending seismic profile across the headwall scarp of the Gorgon Slide and the reconstructed (i.e. pre-failure) seabed. D: Isopach

between reconstructed pre-failure seabed depth-structure map, assuming minimum extent of the headwall scarp.

Figure 4. A: World distribution of documented slides in peer-reviewed literature, containing information on evacuated (Ve) and deposited (Vd) volumes. Note that the Gorgon Slide as the only carbonate-dominated slide. B: Vd/Ve ratio of the submarine landslide in (A).

FIGURE 1

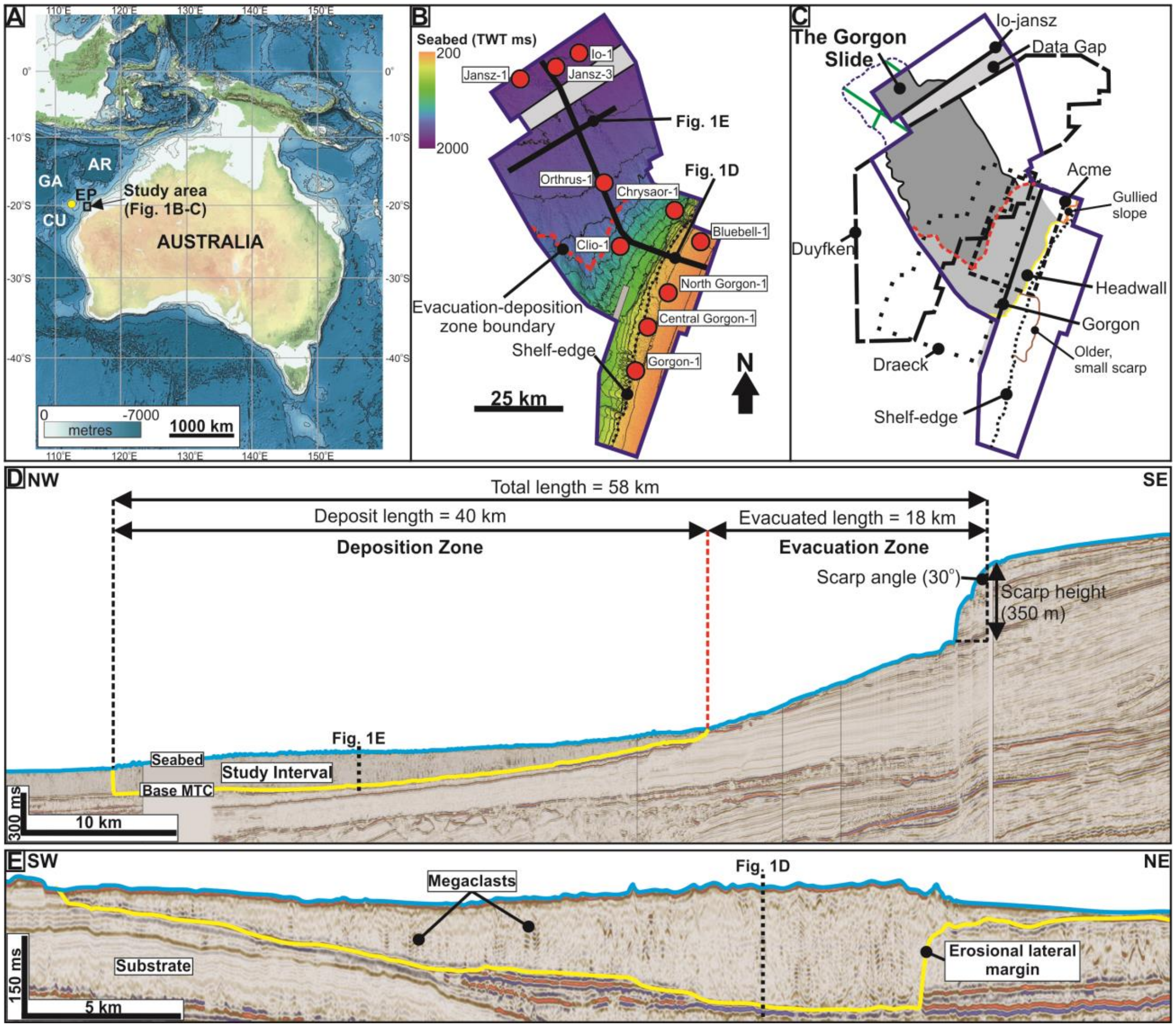
A
110°E
120°E
130°E
140°E
150°E
0°
-10°S
-20°S
-30°S
-40°S
AR
GA
EP
CU
Study area
(Fig. 1B-C)
AUSTRALIA
0
-7000
metres
1000 km
B
Seabed (TWT ms)
200
2000
Io-1
Jansz-1
Jansz-3
Fig. 1E
Fig. 1D
Orthrus-1
Chrysaor-1
Bluebell-1
Clio-1
North Gorgon-1
Central Gorgon-1
Gorgon-1
Evacuation-deposition
zone boundary
Shelf-edge
25 km
N
C
The Gorgon
Slide
Io-jansz
Data Gap
Acme
Gullied
slope
Duyfken
Headwall
Gorgon
Older,
small scarp
Draeck
Shelf-edge
D NW
SE
Total length = 58 km
Deposit length = 40 km
Evacuated length = 18 km
Deposition Zone
Evacuation Zone
Scarp angle (30°)
Scarp height
(350 m)
Fig. 1E
Seabed
Study Interval
Base MTC
300 ms
10 km
E SW
NE
Fig. 1D
Megaclasts
Substrate
Erosional lateral
margin
150 ms
5 km

344 FIGURE 2

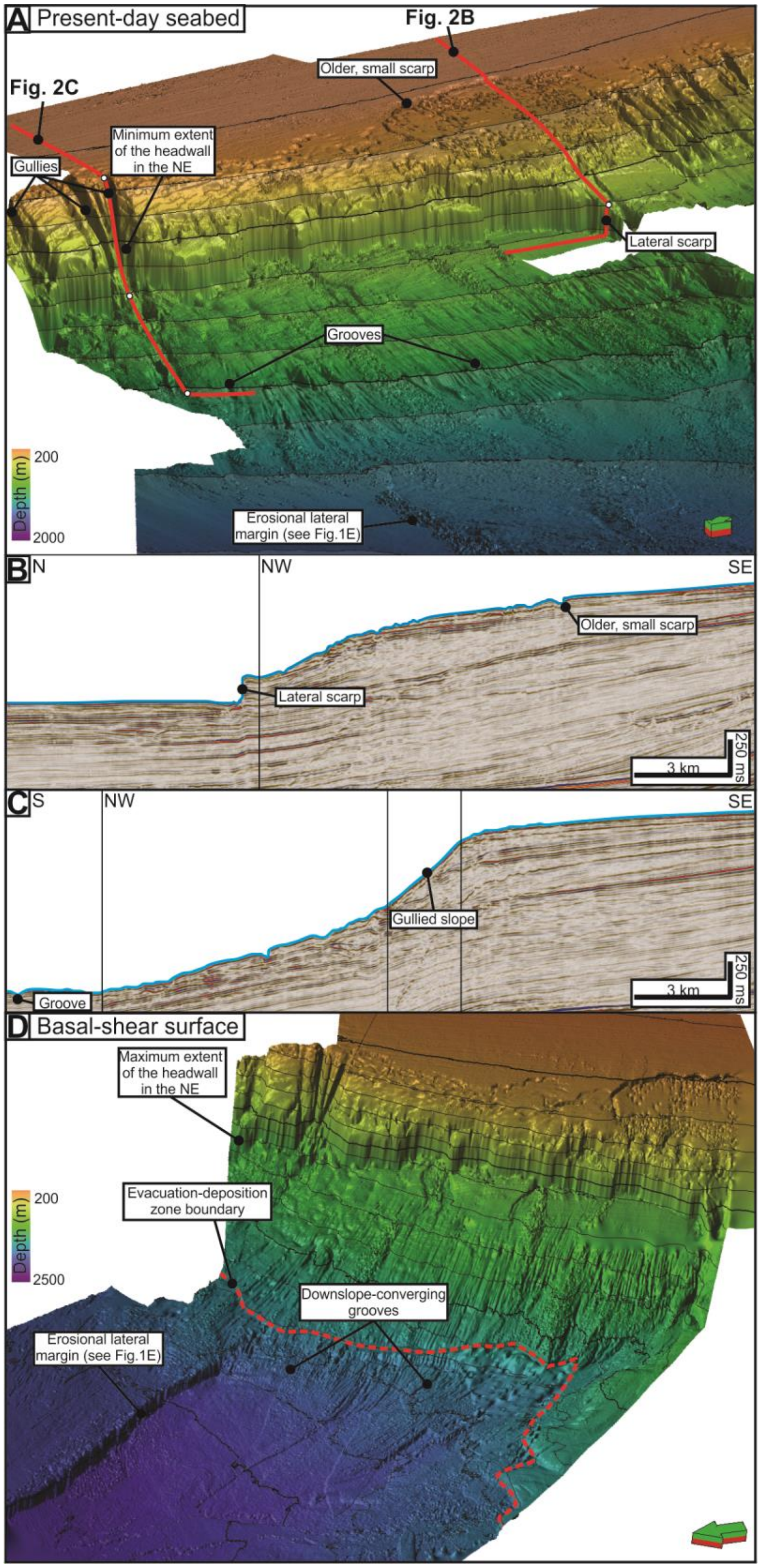

345

346 FIGURE 3

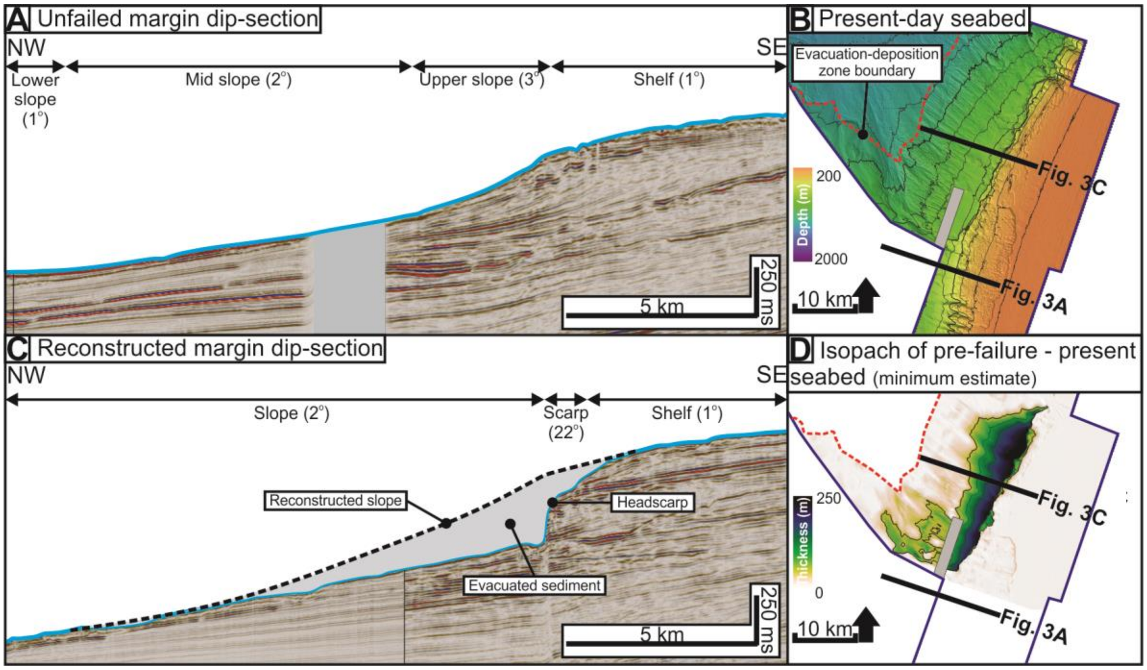

347

FIGURE 4

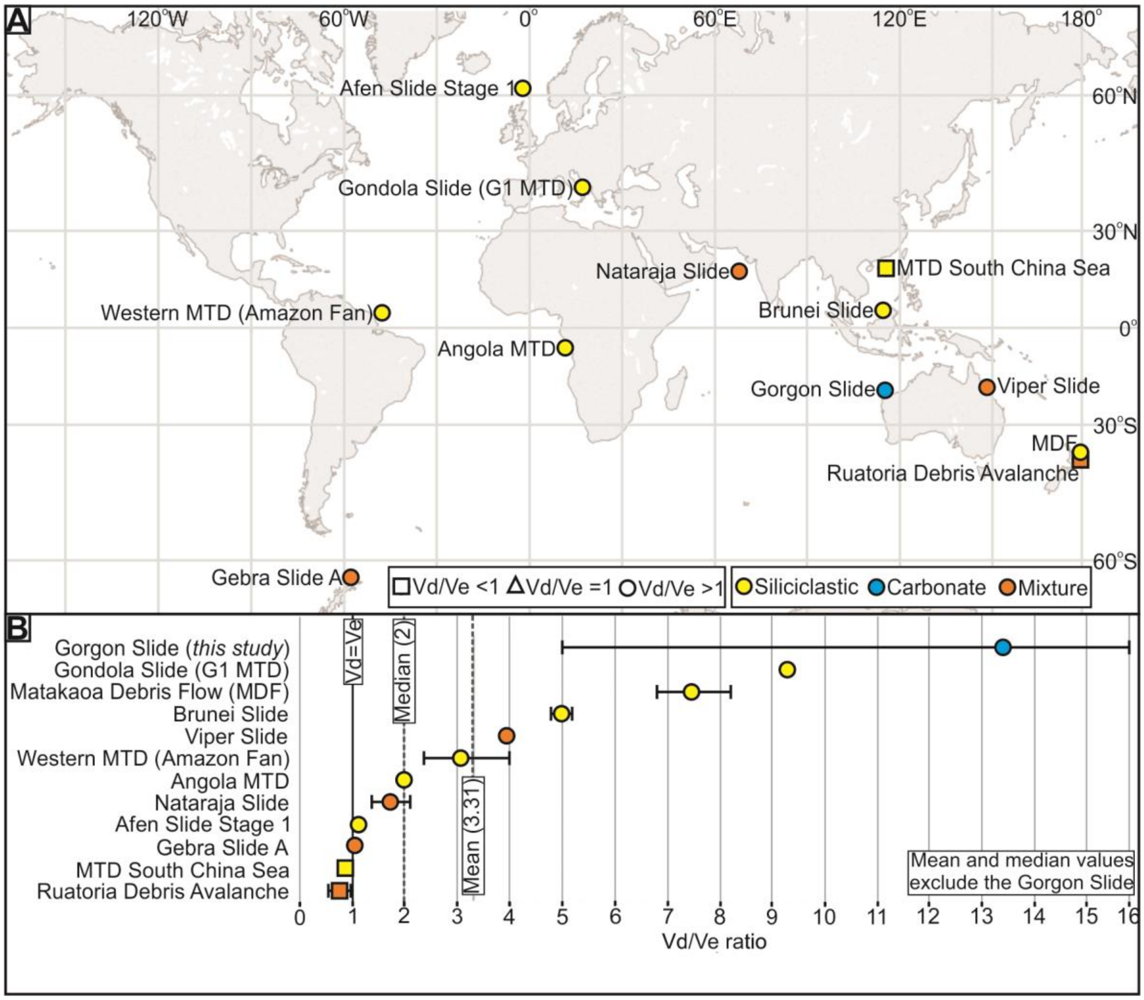
A
120°W
60°W
0°
60°E
120°E
180°
60°N
30°N
0°
30°S
60°S
Afen Slide Stage 1
Gondola Slide (G1 MTD)
Nataraja Slide
MTD South China Sea
Brunei Slide
Western MTD (Amazon Fan)
Angola MTD
Gorgon Slide
Viper Slide
MDF
Ruatoria Debris Avalanche
Gebra Slide A
Vd/Ve <1 Vd/Ve =1 Vd/Ve >1
Siliciclastic Carbonate Mixture
B
Gorgon Slide (*this study*)
Gondola Slide (G1 MTD)
Matakaoa Debris Flow (MDF)
Brunei Slide
Viper Slide
Western MTD (Amazon Fan)
Angola MTD
Nataraja Slide
Afen Slide Stage 1
Gebra Slide A
MTD South China Sea
Ruatoria Debris Avalanche
Vd=Ve
Median (2)
Mean (3.31)
Mean and median values exclude the Gorgon Slide
0 1 2 3 4 5 6 7 8 9 10 11 12 13 14 15 16
Vd/Ve ratio